International Journal of Microwave and Wireless Technologies

cambridge.org/mrf

A novel compact quad-band planar antenna using meander-line, multi-stubs, and slots for WiMAX, WLAN, LTE/5G sub-6 GHz applications

Tarek Maamria[1], Mouloud Challal[2], Fateh Benmahmoud[1], Khelil Fertas[2] and Ammar Mesloub[1]

[1]Antennas and Microwave Devices Laboratory, Polytechnic Military School, Bordj El Bahri, 16111 Algiers, Algeria and [2]Signals and Systems Laboratory, Institute of Electrical and Electronic Engineering, University M'hamed BOUGARA of Boumerdes, Boumerdes, Algeria

Research paper

Cite this article: Maamria T, Challal M, Benmahmoud F, Fertas K, Mesloub A (2023). A novel compact quad-band planar antenna using meander-line, multi-stubs, and slots for WiMAX, WLAN, LTE/5G sub-6 GHz applications. *International Journal of Microwave and Wireless Technologies* **15**, 852–859. https://doi.org/10.1017/S1759078722000939

Received: 7 March 2022
Revised: 17 July 2022
Accepted: 18 July 2022

Key words:
compact multiband antenna; meander-line; multi-stubs; inverted L-shaped; Sub-6 GHz 5G

Author for correspondence:
Tarek Maamria,
E-mail: maamria.tarek@gmail.com

Abstract

This article concerns the design of a new quad-band monopole antenna with a specific configuration and reduced size. The antenna design is based on a single step meander-line parasitic structure, parasitic stubs, and double inverted L-shaped defected microstrip structure units on the top side of the substrate, and double rectangular-shaped defected ground structure units along with partial ground plane on the bottom side. This design procedure allows to achieve quad-band characteristics and improve the impedance matching. The fabricated antenna prototype with overall dimensions of $(0.24\lambda_0 \times 0.17\lambda_0 \times 0.013\lambda_0)$ is operating at 2.55, 3.65, 4.65, and 5.8 GHz with fractional bandwidth about 7.7, 12.84, 9.23, and 12.8%, respectively. The antenna exhibits an omnidirectional and a monopole like radiation patterns in the H- and E-planes, respectively, with suitable gains between 2.1 and 3.75 dBi. The measurement results are in good agreement with simulation values, which indicates that the proposed antenna design is suitable for WiMAX, LTE B7 (2.52–2.75 GHz), Sub-6 GHz 5G (n77) (3.39 – 3.87 GHz), Sub-6 GHz 5G (n78) (4.4–4.86 GHz), and WLAN, LTE B46 (5.1–5.82 GHz) wireless applications.

Introduction

Antennas for wireless communication systems have played an important role in every sector. The demand for compact and multiband antennas is growing due to the newly expanding microwave and mobile communication systems [1], such as that used in 5G base stations and mobile phones. This exhaustive use of the radio-electric spectrum has generated a great interest in devices, making it possible to cover several bands simultaneously. The 5G spectrum covers from sub-6 GHz up to millimeter-wave frequencies. For civil, military, satellite, and underwater applications, the 5G antenna should be operated at wide and/or multiple frequency bands. Due to the disparity of the frequency band, antennas designed for a 5G communication system face enormous challenges. The antenna for 5G must be compacted enough to be implanted in portable devices [2]. Moreover, as the sub-6 GHz antenna has to work along with the current long-term evolution LTE and other service bands, the 5G antenna should cover the sub-6 GHz bands and the existing WiMAX, WLAN, and LTE bands. Among different categories of antenna. Microstrip patch antenna becomes the appropriate optimal due to their attractive low-profile features, lightweight, inexpensive, and easy integration [3].

On the other hand, different techniques have been reported to achieve multiband compact antennas [4–6]. Authors in [5] proposed a non-conventional multiband patch antenna design based on a Genetic Algorithm with a filtering aspect. Based on different fundamental steps, the developed script was performed to achieve good impedance bandwidth in frequency bands [3.7/5.5 and 7.2 GHz] that correspond to WiMAX/WLAN and X-band standards, respectively. In [6] and [7] it was examined that the miniaturized antennas were based on Slot structure, and slit loading techniques. In [8], a modified rectangular patch antenna with U-shaped defected ground structure (DGS) unit and two parasitic elements for WLAN, WiMAX, C, and X bands applications were described. The application of metamaterials to improve the performance of small antennas has been reported in many published works. In [9], a metasurface composed of pairs of nonuniform cut wires with different lengths is proposed to reduce the mutual coupling of an extremely compact dual-band two-element MIMO antenna array. The isolation between two patch antennas with the edge-to-edge spacing of only 0.008 wavelengths can be enhanced to more than 25 dB at both 2.6 and 3.5 GHz bands. In [10], a miniaturized multiband antenna for Bluetooth, WLAN, WiMAX, LTE, and X band applications was reported. In [11], a planar antenna for a 5G mobile terminal operating at sub-6 GHz was presented. The antenna consists of three ground strips and a driven strip which has a –

6 dB impedance bandwidth of 700–960 MHz and 1.6–5.5 GHz. However, a large ground plane of 135×80 mm^2 is required. An ellipse-shaped patch antenna for LTE-R and 5G mid-band was described in [12]. With an overall dimension of 180×60 mm^2, the developed antenna has a dual band response of 660–790 MHz and 3.28–3.78 GHz. A dual-polarized magneto-electric dipole antenna for 5G communication applications was reported in [13]. The investigated antenna is made up of four horizontal fishtail-shaped patches and four vertical patches that are shorted to the ground. With an overall dimension of 150×150 mm^2, the antenna achieved an operational band of 3.05–4.42 GHz. However, it does not cover the N79 for the 4.4–5 GHz range. A monopole antenna for 4G/5G applications was introduced in [14]. The investigated single-element antenna achieves operating bands of 1.24–2.64 and 3.34–5 GHz. Nevertheless, because of its large size of 150×80 mm^2, it cannot cover the N79 band. A planar antenna for 2G/3G/4G/5G sub-6 GHz applications was reported in [15]. A −6 dB impedance bandwidth of 2.5–4.8 GHz with a dimension of 50×19.75 mm^2 was obtained. However, a large ground plane of 110×50 mm^2 is required. In [16], an UWB antenna for 5G lower band application was described. With an overall dimension of 80×50 mm^2, the examined design was able to function in the 2.32–5.24 GHz range. In [17], a differential fed frequency reconfigurable antenna for mid-band 5G applications was presented. The developed antenna uses two different substrates, and the reconfigurability was achieved via four PIN diodes. The examined antenna, with an overall volume of $100 \times 100 \times 5.7$ mm^3, achieved dual operating bands of 2.37–2.67 and 3.39–3.62 GHz. Its 3D shape, however, limits its application in mobile devices. Besides, it does not cover the whole sub-6 GHz 5G spectrum. In [18], a four-port MIMO antenna for 5G applications was investigated. The exhibited antenna, printed on a 5016:0650 mm^2 substrate, can only cover a 3.4–3.8 GHz frequency range. A dual-band MIMO antenna for mid-band 5G wireless applications was published in [19]. Also, in [20], a dual-band with an enhanced impedance using a tapered slot is designed and studied. The antenna presents a very large frequency ratio, making it very suitable for integrated 4G/millimeter-wave, 5G, and beyond 5G applications. Two-antenna pairs are arranged vertically on two sides of the ground plane to produce dual bands of 3.4–3.6 and 4.8–5 GHz. Although many of the reported antennas accomplished wide/multiple operating bands [21–23], their 3D profile has a complicated geometry, making it hard to realize. Furthermore, some of the suggested designs partially cover the sub-6 GHz band. In this paper, a novel multiband compact antenna is proposed. The antenna is printed on FR-4 dielectric substrate with thickness of 1.5 mm, relative dielectric constant of 4.3, and loss tangent of 0.025. The simulated and measured return loss and radiation patterns are presented and discussed. The tested antenna provides acceptable results in terms of reflection coefficient and radiation patterns indicating that it is well-suited for 5G Sub-6 GHz (n77 / n78), WLAN, WiMAX, and LTE (B7/B46) wireless applications [24]. The target bands are summarized in Table 1.

Table 1. Required frequency bands for the proposed antenna [18]

Band	Frequency, GHz
LTE B7 / WiMAX (IEEE 802.16e)	2.52–2.75
LTE B46 / WLAN (IEEE 802.11a)	5.1–5.82
Sub-6 GHz 5G (n77)	3.39–3.87
Sub-6 GHz 5G (n78)	4.4–4.86

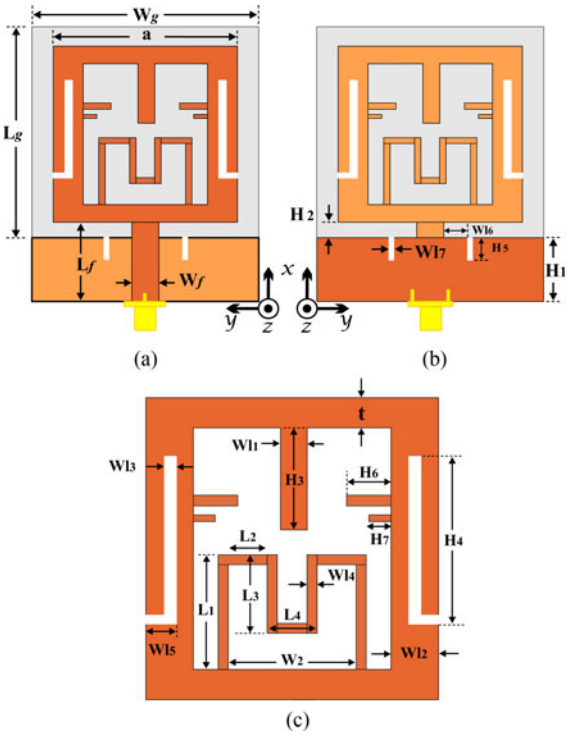

Fig. 1. Geometry of the proposed antenna: (a) front view; (b) back view, and (c) patch view.

Antenna structure and design procedure

The configuration of the proposed antenna is shown in Fig. 1 whereas the geometrical dimensions are listed in Table 2. It consists of a single-step meander-line parasitic structure, parasitic stubs, and double inverted L-shaped defected microstrip structure (DMS) units on the top side of the substrate and double rectangular-shaped DGS units along with partial ground plane on the bottom side.

The step-by-step design evolution of the proposed antenna is shown in Fig. 2. Firstly, a square-ring metallic patch and a partial ground plane, operating at 3.5 GHz, is designed, using full-wave electromagnetic CST microwave simulator, denoted as reference antenna (Ant 0) as shown in Fig. 2(a). The total antenna footprint is 28×19 mm^2. The design process is inspired from [25].

The resonant frequency of the square-ring metallic patch can be estimated with the following formula [26]:

$$f_n = \frac{nc}{4a\sqrt{\varepsilon_{eff}}} \quad n = 1, 2, 3 \ldots \tag{1}$$

where c is the speed of electromagnetic wave in free space, a represents the side length of the square ring, ε_{eff} is the equivalent permittivity of the substrate, and n is the integer representing index of the antenna's operating mode. In this paper, the first resonance is 1/4 wavelength, this is equal to the length of the ring from the base to top that is, total ring length/2. As, $f = 3.5$ GHz. The simulated $|S_{11}|$ result of this antenna is illustrated in Fig. 3 In order to obtain the desired dual-band operation with good impedance

https://doi.org/10.1017/S1759078722000939 Published online by Cambridge University Press

Table 2. Geometrical dimensions of the proposed antenna

Parameter	Value (mm)	Parameter	Value (mm)
W_g	19	WL_1	0.5
L_g	19.8	WL_2	0.8
W_f	2.2	WL_3	0.4
L_f	5.2	WL_4	0.3
H_1	8.2	WL_5	0.6
H_3	5.2	t	0.8
H_4	11.2	a	14
L_4	0.7	L_1	7.8

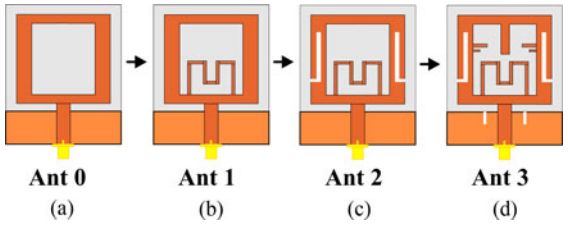

Fig. 2. Evolution procedure of the proposed antenna geometry.

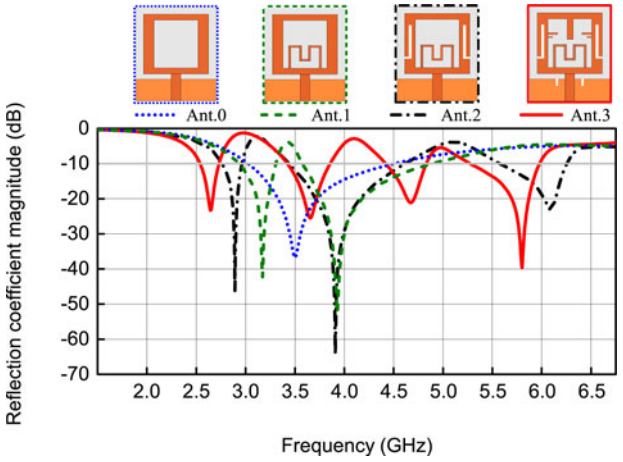

Fig. 3. Reflection coefficient magnitude versus frequency for different antenna structures.

matching, the next step consists of embedding a single-step meander-line parasitic structure into the bottom center of the square-ring antenna as illustrated in Fig. 2(b). This antenna, operates at 3.2 and 3.9 GHz, is referred as Ant 1. The length for this resonance can be calculated as [27]:

$$L_{res2} = \sum_{i=1}^{n} L_i + t + L_f - H_1(\sim 0.5\lambda_{3.65\,\mathrm{GHz}}). \tag{2}$$

Hence,

$$f_{r2} = \frac{c}{2L_{res2}\sqrt{\varepsilon_{eff}}} \approx 3.65\ \mathrm{GHz}, \tag{3}$$

where

$$\varepsilon_{eff} = \frac{\varepsilon + 1}{2}. \tag{4}$$

The meandered line enhances the effective current path which facilitates the compactness of the structure. This method is generally used in wired antennas [28]. Finally, two further steps are added in the design process to achieve the final antenna. The generation of three distinct frequencies (2.8, 3.9, and 6.2 GHz) is obtained when adding double inverted L-shaped DMS units on the patch, denoted as Ant 2, and then to support more wireless standards in a single antenna design, the generation of four distinct frequencies (2.55, 3.65, 4.55, and 5.8 GHz) is achieved when adding five opens stubs along with double rectangular-shaped DGS units, denoted as Ant 3, as illustrated in Fig. 2(d). The addition of double inverted L-shaped DMS units generates a discontinuity in the square ring antenna. Due to this discontinuity, the surface electrical current length increases [29]. This increase in current path length impacts the antenna's input impedance, which tends the antenna to exhibit additional resonance. The length of the slot is provided by equation (5)

$$L_{res3} = H_4 + WL_5 + t + L_f - H_1(\sim 0.5\lambda_{4.65\,\mathrm{GHz}}). \tag{5}$$

To examine more the operating mechanism of the presented antenna, namely Ant 3, the surface current density distribution on the patch surface (top view) and ground plane (bottom view) of the proposed antenna is simulated at 2.55, 3.65, 4.65, and 5.8 GHz resonant frequencies as shown in Fig. 4. It can be seen that, at the first resonant frequency, the surface current density is mostly concentrated in the inner vertical metallic strips of the square-ring patch along with the double inverted L-shaped DMS units. At the second resonant frequency, the surface current density is mainly focused near the meander-line parasitic structure ($J_1 - J_4$, and $J_5 - J_8$). At the third resonant frequency, the current density is more concentrated in the double inverted L-shaped DMS units ($J_9 - J_{13}$, and $J_{14} - J_{18}$) having an electrical length of $0.5\lambda_{4.65\,\mathrm{GHz}}$, formed by WL_3, and H_4, as indicated in Fig. 4(e). At the fourth resonant frequency, the current density is mainly focused in the stub ($J_{19} - J_{20}$, and $J_{21} - J_{22}$) along with the double rectangular-shaped DGS units ($J_{23} - J_{26}$, and $J_{27} - J_{30}$), as indicated in Figs 4(g) and 4(h), respectively. It can be noticed that it is difficult to isolate the exact areas responsible for the resonances, especially at the third and fourth frequencies, as the different elements interact with each other. The surface current density around the contours of a vertical stub is higher at 5.8 GHz, contributing to impedance matching around 5.8 GHz as observed from the reflection coefficient plot for step 4, shown in Fig. 3. The variations of the real and imaginary parts of the antenna input impedance Z_{11} are shown in Fig. 5. From the figure, it can be concluded that the real and imaginary parts of Z_{11} are close to 50 and 0 Ω, respectively, over the four resonant frequency bands, which gives a good impedance matching and confirms the result in Fig 3.

Parametric studies

In order to ensure that the proposed antenna performance could meet the desired bands, parametric studies are carried out in this section. The effect of varying the width of square-ring "a", length

https://doi.org/10.1017/S1759078722000939 Published online by Cambridge University Press

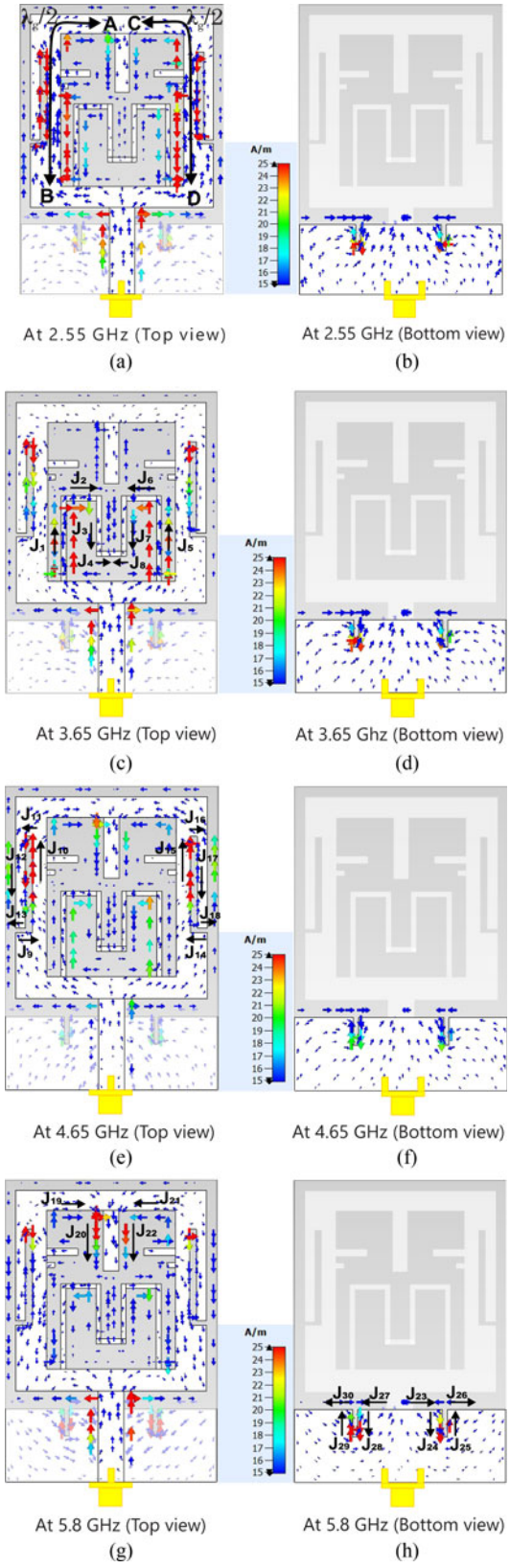

Fig. 4. Surface current distribution on the radiating patch and modified ground plane of the proposed antenna at 2.55, 3.65, 4.65, and 5.8 GHz resonant frequencies.

of the meander line $(L_1 + L_2)$, length of L-shaped slot $(H_4 + Wl_5)$, and length of a shorting oblique stub H_3 and width W_3 are investigated as shown in Figs 6–9, respectively.

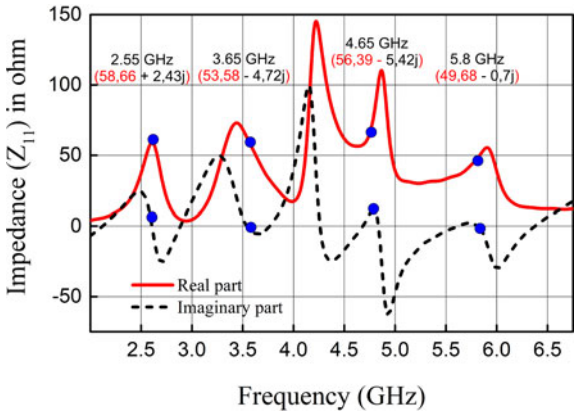

Fig. 5. Variations of the real and imaginary parts of the antenna input impedance Z_{11}.

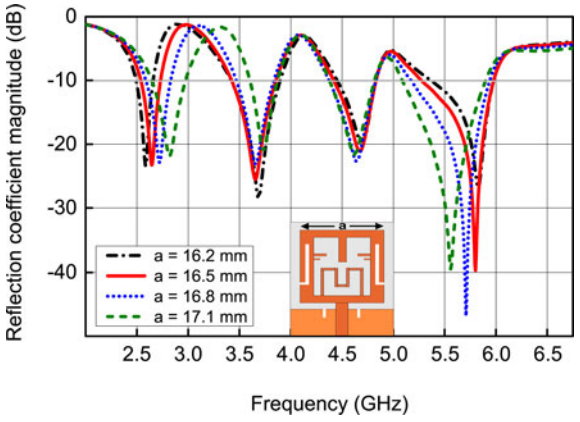

Fig. 6. Effect of varying the square-ring width *a*.

Effect of varying the square-ring width a

The effect of the width "*a*" is investigated, while the other parameters are kept constant as shown in Fig. 6. The simulation is carried out for "*a*" values of 16.2, 16.5, 16.8, and 17.1 mm. Figure 6 shows that the 2.55 and 5.8 GHz resonant frequencies depend on the parameter "*a*". The variation in the value of (*a*) from 16.2 to 17.1 mm lead to shift up the lower resonance frequency from 2.55 to 2.8 GHz. Main while, it shift down of the upper resonance frequency from 5.8 to 5.51 GHz.

Influence of the variation of the meander-line length

Figure 7 demonstrates the effect on the reflection coefficient when the parameter $(L_1 + L_2)$ is varied from 12.2 to 13.7 mm. An increase in length $(L_1 + L_2)$of the meander line leads to shift up of the resonant frequencies (except the first one).

Varying the L-shaped slot length

Similarly, the influence of the L-shaped slot length $(H_4 + Wl_5)$ on the reflection coefficient is given in Fig. 8. It can be seen from the figure below that as the length $(H_4 + Wl_5)$ increases, the reflection coefficient at the frequency 4.65 GHz shifts toward the lower frequency side. Hence, a value of 10 mm for sub-6 GHz 5G

https://doi.org/10.1017/S1759078722000939 Published online by Cambridge University Press

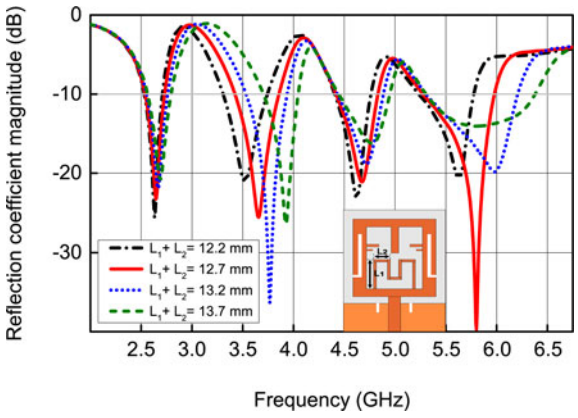

Fig. 7. Effect of varying the meander-line length $L_1 + L_2$.

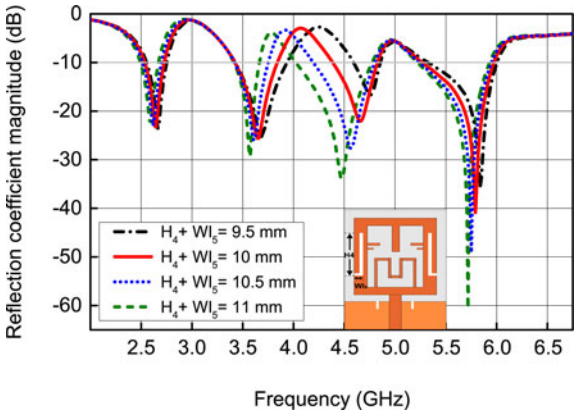

Fig. 8. Effect of varying the L-shaped slot length.

frequency bands (n79) is considered to get the third resonant frequency at 4.65 GHz.

Effect of varying the open stubs lengths

Figure 9 shows the antenna return loss $|S_{11}|$ for different values of length $(H_3 + W_3)$. The increase in the length of the stubs leads to shifting of the third and fourth resonant frequencies to lower frequencies, while the first and second resonant frequencies are kept unchanged, a value of 7.5 mm is considered.

Fabrication and measurements

A prototype of the designed antenna was fabricated and tested to validate the proposed design. A photograph of the fabricated structure is shown in Fig. 10(a). The *S* parameters were measured using a vector network analyzer ZNB20. The far-field radiation patterns of the principal planes (E and H) were measured in a fully equipped anechoic chamber as shown in Fig. 10(b), where the commercial Logarithmic Periodic Antenna (HyperLOG 30180) is used as a reference antenna, at output power of 10 mW (10 dBm). The distance between the transmitting and receiving antennas is $d = 1$ m.

The obtained measured results are compared to the simulation ones as indicated in Fig. 11. This figure clearly confirms the quad-band behavior of the proposed antenna [2.52–2.75 GHz], [3.39–

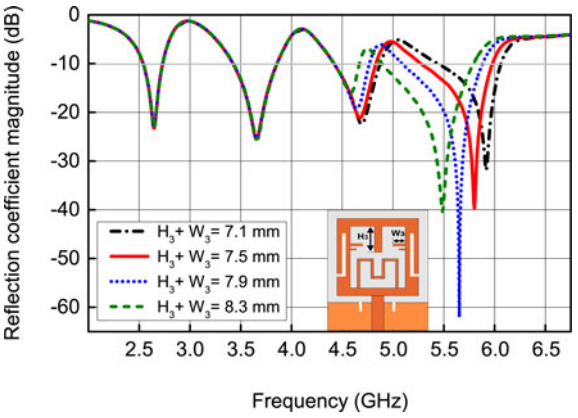

Fig. 9. Effect of varying the length of the open stubs.

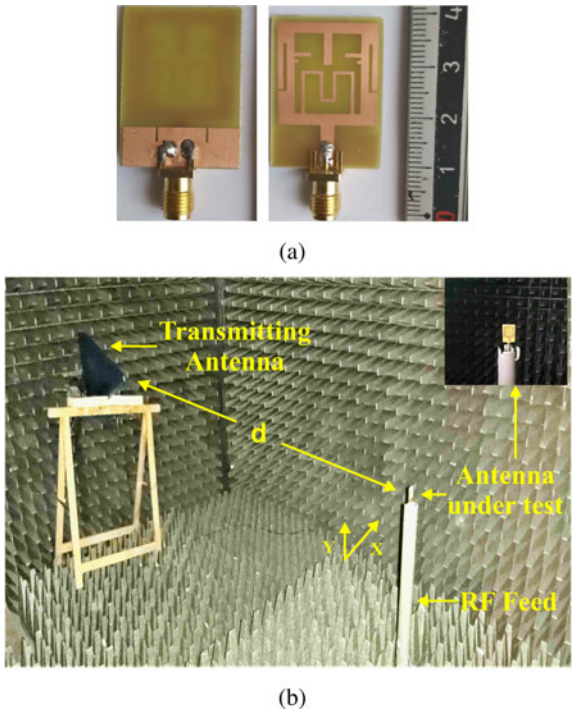

Fig. 10. Fabricated antenna and measurement setup. (a) Photograph of the proposed antenna, and (b) antenna measurement in an anechoic chamber.

3.87 GHz], [4.4–4.86 GHz], and [5.2–6 GHz] covering the 5G sub-6 GHz (n78/n79) at (3.65/4.65 GHz), and LTE bands (B7/B46) at (2.55/5.8 GHz). Moreover, the two compared results present an acceptable agreement; however, the insignificant disagreement is due to errors in the fabrication and measurement apparatus.

The simulated and measured realized gains are shown in Fig. 12(a) where the simulated radiation efficiency is depicted in Fig. 12(b). The antenna's realized gain is 2.1, 3.15, 3.35, and 3.75 dBi in the first, second, third, and fourth bands, respectively. The radiation efficiency is about 82, 85, 76, and 73% in the first, second, third, and fourth bands, respectively.

Figure 13 shows the simulated and measured 2D radiation patterns in two principal planes – namely, the $E-(xz)$ and $H-(xy)$ planes for four resonant frequencies of 2.55, 3.65, 4.65, and 5.8 GHz. At lower frequencies, the antenna exhibits omni-directional

https://doi.org/10.1017/S1759078722000939 Published online by Cambridge University Press

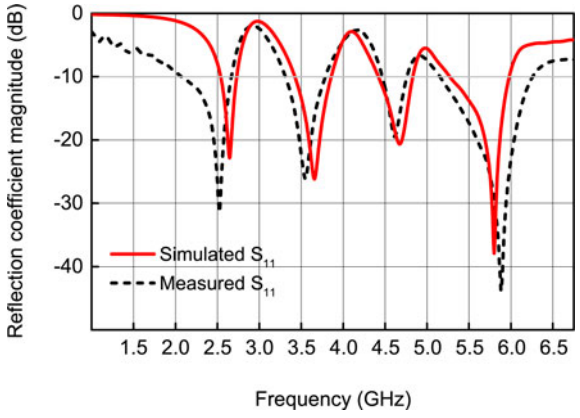

Fig. 11. Simulated and measured reflection coefficient magnitude of the proposed antenna.

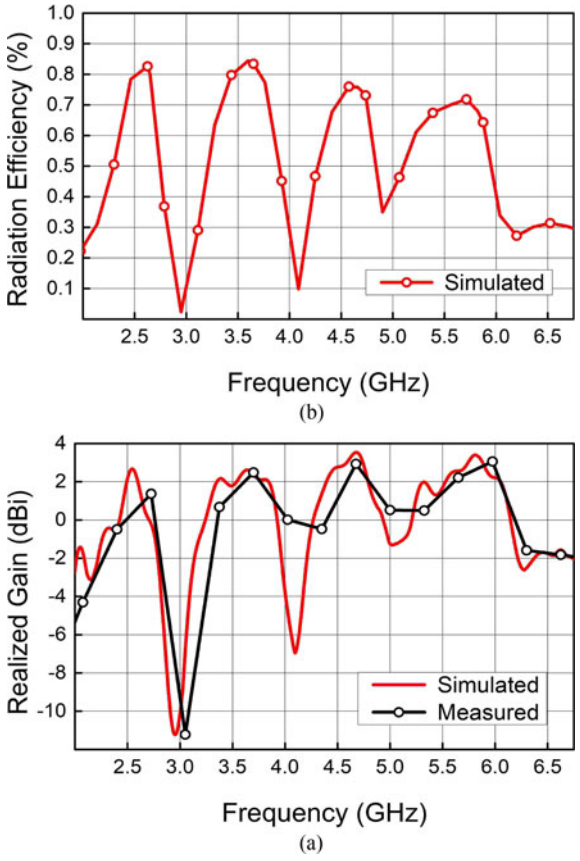

Fig. 12. Antenna's performance in terms of (a) realized gain, and (b) radiation efficiency.

patterns for H-plane and a donut shape for E-plane with a low cross-polarization field and patterns are about the same as that of a typical monopole antenna. Polarization purity can only be seen at low frequencies where the cross-to-co polarization ratio is around − 35 dB, in contrast to higher frequencies, where the cross-polarization is dominant especially in H-plane. About 25–40 dB isolation between co-polarized and XP radiations is achieved with the proposed structure.

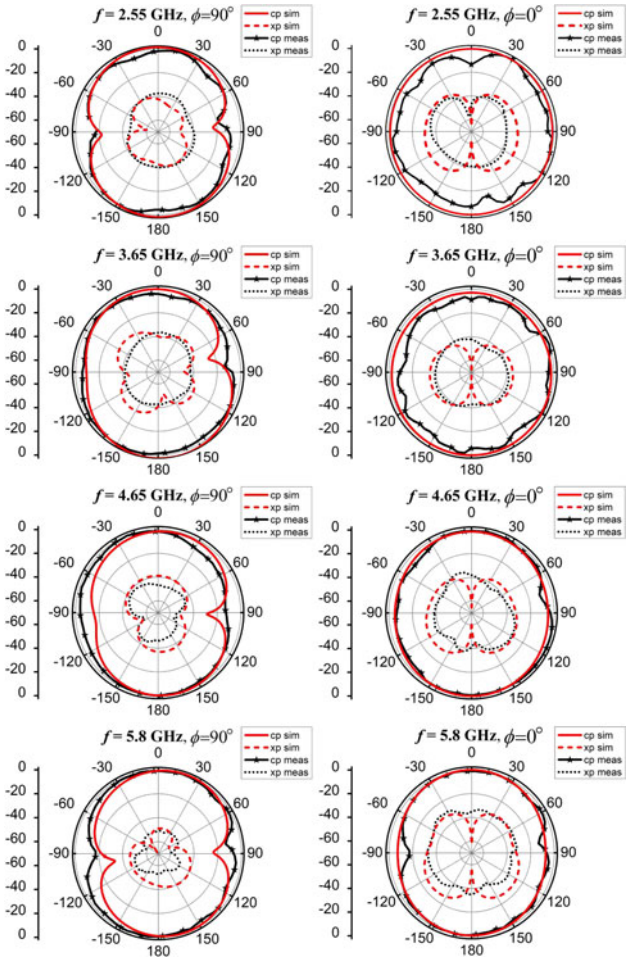

Fig. 13. Simulated and measured radiation patterns of E- and H-planes at 2.55, 3.65, 4.65, and 5.8 GHz (xp, cross-polarization; cp, co-polarization).

Table 3 illustrates a comparison between the proposed structure and recently reported antennas. From this table, the presented antenna is more compact than those described in [15, 17, 30–33] while having wider operating bandwidth adequate to cover all the sub-6 GHz 5G bands. Even though some reported designs achieved high gain and high efficiency, their large size and complex structure limit their applications in portable communications devices [17] and [32]. Moreover, the antennas reported in [30] and [32] did not cover the all-sub-6 GHz bands. Accordingly, these attractive characteristics make the proposed antenna suitable for LTE and 5G sub-6 GHz communication applications.

Conclusion

In this paper, a new compact and miniaturized multi-band planar monopole antenna has been designed, fabricated, and tested. The obtained results in simulation and measurement show a behavior of quad-band and better impedance matching. The presented antenna with compact size of $(0.24\lambda_0 \times 0.17\lambda_0 \times 0.013\lambda_0)$ covers LTE B7 (2.52–2.75 GHz), Sub-6 GHz 5G (n77) (3.39–3.87 GHz), Sub-6 GHz 5G (n78) (4.4–4.86 GHz), and LTE B46 (5.1–5.82 GHz), while it has high radiation efficiency and moderately stable radiation patterns. The proposed quadband antenna operates in all the frequency bands of mobile telecommunication standards

https://doi.org/10.1017/S1759078722000939 Published online by Cambridge University Press

Table 3. Performance comparison with recently published works

References	Total area (mm^2)	Central frequencies (GHz)	Fractional BW (%)	Peak gain (dBi)	Efficiency (%)	Profile and substrate	Method of designing
[15][a]	129.75×50	0.8	14.06	1.8	60	Planar	T-shaped element, one matching
		2.4	2.98	~	~		stub applied with tapering, and
		4	10	2.9	2.9	FR4	meandering techniques
[17][a]	100×100	2.45	6.6	5	6 4.65	3D	Reconfigurable antenna (four PIN
		3.5	11.9	6.8	96.5	FR4	diode switches)
[30]	30×24.8	3.1	5.9	1.35			
		5.52	5.6	1	Not	Planar	Fractal antenna loaded-shaped slot
		7.31	7.3	1.07	specified	FR4	and metamaterial
		9.72	3.02	1.75			
[31][a]	37×35	2	7.4	1			
		2.4	22.43	1.75	>85	Planar	Reconfigurable antenna (lumped
		3.1	29.17	1.98		FR4	element switch)
		3.4	19.54	1.72			
[32]	68×71	0.9	24.47	2.2	65.1	Polyimide	
		2.4	6.99	2.6	86.2	based	Triangular embedded radiators
		3.5	8.69	0.8	95.7	flexible	
[33][a]	36×31	3.29–3.63	10.71	7.17	79.58	Planar	Rectangular slot, inverted stub on
		4.39–5.2	14.15			FR4	upper edge, and folded T-shaped
Proposed work	28×19	2.55	7.7	2.1	82.2		
		3.65	12.84	3.15	85.1	Planar	Rectangular stub/two rectangular
		4.65	9.23	3.35	76.3	FR4	rings, and L-shaped slot
		5.8	12.8	3.67	73.1		

[a]Only sub-6 GHz band is considered for comparison.

4G (B7/B46), and 5G (n77/n78), and other applications, including WLAN and WiMAX.

Acknowledgements. The authors thank the Dean of the Faculty of Electric Engineering, University of Science and Technology–Houari Boumediene, Algiers and Anechoic laboratory staff of that Faculty.

Conflict of interest. The authors declare that they have no known competing financial interests or personal relationships that could have appeared to influence the work reported in this paper.

References

1. **MA Matin** (Ed.). (2021) *Wideband, Multiband, and Smart Antenna Systems*. Switzerland: Springer.
2. **M Fallahpour and R Zoughi** (2017) Antenna miniaturization techniques: a review of topology-and material-based methods. *IEEE Antennas and Propagation Magazine* **60**, 38–50.
3. **CA Balanis** (2005) *Antenna Theory: Analysis and Design*. New Jersey: John wiley and sons, pp. 811–876.
4. **FA Konkyana, B Lalitha and BA Sudhakar** (2019) A review on microstrip antennas with defected ground structure techniques for ultra-wideband applications. In: 2019 International Conference on Communication and Signal Processing (ICCSP). IEEE, pp. 0930–0934.
5. **K Fertas, S Tebache, F Ghanem, S Tedjini and R Aksas** (2020) Non-conventional multiband patch antenna design with filtering aspect based on genetic algorithm. *IETE Journal of Research* **66**, 815–822.
6. **F Fertas, M Challal and K Fertas** (2020) A compact slot-antenna with tunable-frequency for WLAN, WiMAX, LTE, and X-band applications. *Progress In Electromagnetics Research C* **102**, 203–212.
7. **SM Haque and KM Parvez** (2017) Slot antenna miniaturization using slit, strip, and loop loading techniques. IEEE Transactions on Antennas and Propagation, pp. 2215–2221.
8. **A Boutejdar, M Challal, SD Bennani, F Mouhouche and K Djafri** (2017) Design and fabrication of a novel quadruple-band monopole antenna using a U-DGS and open-loop-ring resonators. *Advanced Electromagnetics* **6**, 59–63.
9. **F Liu, J Guo, L Zhao, GL Huang, Y Li and Y Yin** (2019) Dual-band metasurface-based decoupling method for two closely packed dual-band antennas. *IEEE Transactions on Antennas and Propagation* **68**, 552–557.
10. **F Fertas, M Challal and K Fertas** (2020) Miniaturized quintuple band antenna for multiband applications. *Progress In Electromagnetics Research M* **89**, 83–92.
11. **Z An and M He** (2020) A simple planar antenna for sub-6 GHz applications in 5G mobile terminals. *The Applied Computational Electromagnetics Society Journal (ACES)* **35**, 10–15.
12. **AK Arya, SJ Kim and S Kim** (2020) A dual-band antenna for LTE-R and 5G lower frequency operations. *Progress In Electromagnetics Research Letters* **88**, 113–119.
13. **JN Sun, JL Li and L Xia** (2019) A dual-polarized magneto-electric dipole antenna for application to N77/N78 band. *IEEE Access* **7**, 161708–161715.

https://doi.org/10.1017/S1759078722000939 Published online by Cambridge University Press

14. **M Khalifa, L Khashan, H Badawy and F Ibrahim** (2020) Broadband printed-dipole antenna for 4G/5G smartphones, in Journal of Physics: Conference Series, Vol. 1447, No. 1, 012049, IOP Publishing.
15. **N Sekeljic, Z Yao and HH Hsu** (2019) 5G broadband antenna for sub-6 GHz wireless applications. In 2019 IEEE International Symposium on Antennas and Propagation and USNC-URSI Radio Science Meeting, pp. 147–148.
16. **X Tang, Y Jiao, H Li, W Zong, Z Yao, F Shan and S Gao** (2019) Ultra-wideband patch antenna for sub-6 GHz 5G communications. In 2019 International Workshop on Electromagnetics: Applications and Student Innovation Competition iWEM, pp. 1–3.
17. **G Jin, C Deng, J Yang, Y Xu and S Liao** (2019) A new differentially-fed frequency reconfigurable antenna for WLAN and sub-6 GHz 5G applications. *IEEE Access* **7**, 56539–56546.
18. **S Saxena, BK Kanaujia, S Dwari, S Kumar and R Tiwari** (2018) MIMO antenna with built-in circular shaped isolator for sub-6 GHz 5G applications. *Electronics letters* **54**, 478–480.
19. **Z Ren and A Zhao** (2019) Dual-band MIMO antenna with compact self-decoupled antenna pairs for 5G mobile applications. *IEEE Access* **7**, 82288–82296.
20. **K Sultan, M Ikram and N Nguyen-Trong** (2022) A multiband multibeam antenna for sub-6 GHz and mm-wave 5G applications. *IEEE Antennas and Wireless Propagation Letters* **21**, 1278–1282.
21. **F Benmahmoud, P Lemaitre-Auger and S Tedjini** (2022) Compact wideband multi-arm 3-D wire antenna for GNSS applications. *AEU-International Journal of Electronics and Communications* **143**, 154011.
22. **F Benmahmoud and S Tedjini** (2021) Miniaturized 3D multi-segment wire antenna for 5G. In 2021 IEEE International Symposium on Antennas and Propagation and USNC-URSI Radio Science Meeting (APS/URSI), pp. 705–706.
23. **F Benmahmoud, P Lemaitre-Auger and S Tedjini** (2019) Wideband circularly polarized 3D wire antenna for Wi-MAX applications. In 2019 IEEE-APS Topical Conference on Antennas and Propagation in Wireless Communications (APWC), pp. 250–252.
24. **JT Penttinen** (2019) *5G Explained: Security and Deployment of Advanced Mobile Communications*. Hoboken, NJ: John Wiley.
25. **J Premalatha and D Sheela** (2020) Compact four-port vertically polarized UWB monopole antenna for MIMO communications. Circuit World.
26. **J Yuan, S Wu, Z Chen and Z Xu** (2019) A compact low-profile ring antenna with dual circular polarization and unidirectional radiation for use in RFID readers. *IEEE Access* **7**, 128948–128955.
27. **M Kumar and V Nath** (2020) Design and development of triple-band compact ACS-fed MIMO antenna for 2.4/3.5/5 GHz WLAN/WiMAX applications. *Analog Integrated Circuits and Signal Processing* **103**, 461–470.
28. **Y Rahmat-Samii and E Topsakal** (2021) *Antenna and Sensor Technologies in Modern Medical Applications*. Wiley-IEEE.
29. **T Ali, AM Saadh, RC Biradar, J Anguera and A Andújar** (2017) A miniaturized metamaterial slot antenna for wireless applications. *AEU-International Journal of Electronics and Communications* **82**, 368–382.
30. **T Ali, MS Aw and RC Biradar** (2018) A fractal quad-band antenna loaded with L-shaped slot and metamaterial for wireless applications. *International Journal of Microwave and Wireless Technologies* **10**, 826–834.
31. **S Ullah, I Ahmad, Y Raheem, S Ullah, T Ahmad and U Habib** (2020) Hexagonal shaped CPW feed based frequency reconfigurable antenna for WLAN and sub-6 GHz 5G applications. In 2020 International Conference on Emerging Trends in Smart Technologies (ICETST), IEEE, pp. 1–4.
32. **H Xu, Z Chen, Z Zhao, H Liu and S Zhu** (2021) A flexible and compact tri-band antenna for vehicular wireless video transmission systems. *International Journal of RF and Microwave Computer–Aided Engineering* **31**, e22741.
33. **I Ishteyaq, IS Masoodi and K Muzaffar** (2021) A compact double-band planar printed slot antenna for sub-6 GHz 5G wireless applications. *International Journal of Microwave and Wireless Technologies* **13**, 469–477.

Tarek Maamria received the M.Sc. (Magister) degree in electrical engineering from Polytechnic Military School, Algiers, Algeria, in 2016. Currently, he is a Ph.D. student in the Ecole Militaire Polytechnique of Algiers and his research interests include antenna and RF design, wireless sensors, IoT, and radar cross-section (RCS) of antennas.

Mouloud Challal (M'09–SM'16) received the M.Sc. (Magister) and Doctorate degrees in Telecommunications from National Polytechnic School Algiers and Institute of Electrical and Electronic Engineering (IGEE, ex. INELEC), University M'Hamed BOUGARA Boumerdes (UMBB), ALGERIA, in 2001 and 2012, respectively. He is currently a full professor in the Telecommunications research group, Department of Electronics, and communication systems team leader in the Signals and Systems research Laboratory, IGEE/UMBB; ALGERIA. He handled a lot of responsibilities as Deputy Head of Electronics Department, from 2007 to 2008, Responsible of Master degree program in Telecommunications from 2013 to 2017, Vice-director in charge of studies and students' related issues from 2017 to 2018 and as Director of the IGEE from 2018 to 2021. He was a founding member of the IEEE Algeria Sub-section where he held the post, as a volunteer, of treasurer from 2012 until 2014. He is also among active elements in the creation of both "IEEE Algeria Section" and "Association Algérienne de Génie Électrique et Électronique (AAGEE)". He has authored/co-authored over 95 scientific papers. His current research interests include antennas and RF/microwaves circuits analysis, design and measurement.

Fateh Benmahmoud received the Ing. and M.Sc.A. degrees in electrical engineering from Polytechnic Military School, Algiers, Algeria, in 2015, and the Doctor degree in Optics and Radiofrequencies from the University of Grenoble Alpes, France, in 2020. He participated as jury examiner/opponent for several Master and engineering degree defenses and authored and co-authored over 13 journal papers, letters, or international conferences. Currently, his activity includes antenna systems, wireless sensors, IoT, and signal processing.

Khelil Fertas received the M.Sc. (Magister) and Doctorate degrees in electrical engineering from Polytechnic Military School, Algiers, Algeria and National Polytechnic School, Algiers, ALGERIA in 2014 and 2021, respectively. Currently, he is an assistant professor in the Material School at Algiers and a member of research team at Signals and Systems Laboratory, Institute of Electrical and Electronic Engineering (IGEE, ex. INELEC), University M'Hamed BOUGARA Boumerdes, ALGERIA. His fields of interest include optimization, RF passive and active circuits, DGS behaviors, propagation, and antennas.

Ammar Mesloub received Engineer and Master degree in telecommunications from Polytechnic Military School, Algiers, Algeria, in 2006 and 2009 respectively. He received the Ph.D. in signal processing from EMP. He is an associate professor in Signal Processing Laboratory. His research interests are in signal processing, time-frequency analysis, and time-frequency array signal processing with applications in radar and communications.

https://doi.org/10.1017/S1759078722000939 Published online by Cambridge University Press